

# Modeling the Broadband Spectral Energy Distribution of the Microquasars XTE J1550–564 and H 1743–322

Yongquan Xue<sup>1\*</sup>, Xue-Bing Wu<sup>2†</sup>, Wei Cui<sup>2‡</sup>

<sup>1</sup>*Department of Physics, Purdue University, West Lafayette, IN 47907*

<sup>2</sup>*Department of Astronomy, Peking University, Beijing 100871, P. R. China*

Received 2007

## ABSTRACT

We report results from a systematic study of the spectral energy distribution (SED) and spectral evolution of XTE J1550–564 and H 1743–322 in outburst. The jets of both sources have been directly imaged at both radio and X-ray frequencies, which makes it possible to constrain the spectrum of the radiating electrons in the jets. We modelled the observed SEDs of the jet ‘blobs’ with synchrotron emission alone and with synchrotron emission plus inverse Compton scattering. The results favor a pure synchrotron origin of the observed jet emission. Moreover, we found evidence that the shape of the electron spectral distribution is similar for all jet ‘blobs’ seen. Assuming that this is the case for the jet as a whole, we then applied the synchrotron model to the radio spectrum of the total emission and extrapolated the results to higher frequencies. In spite of significant degeneracy in the fits, it seems clear that, while the synchrotron radiation from the jets can account for nearly 100% of the measured radio fluxes, it contributes little to the observed X-ray emission, when the source is relatively bright. In this case, the X-ray emission is most likely dominated by emission from the accretion flows. When the source becomes fainter, however, the jet emission becomes more important, even dominant, at X-ray energies. We also examined the spectral properties of the sources during outbursts and the correlation between the observed radio and X-ray variabilities. The implication of the results is discussed.

**Key words:** X-rays: binaries — X-rays: individual (XTE J1550–564, H 1743–322) — black hole physics — accretion, accretion discs

## 1 INTRODUCTION

There is growing evidence that the central engine of microquasars is qualitatively similar to that of active galactic nuclei (AGN) or of gamma-ray bursts (GRBs). Collectively, these systems provide an excellent laboratory for studying particle acceleration in the jets of black holes over a vast range of physical scales (Mirabel 2004; Cui 2006). As has been well demonstrated in the study of AGN and GRBs, modelling the broadband spectral energy distribution (SED) of microquasars can be a very effective way to cast light on emission mechanisms and thus on the nature of the central engine. Unlike the cases of AGN and GRBs, however, the availability of such data is highly limited for microquasars, due to the combination of the transient nature of most such sources and the rarity of their outbursting activities (during which they can usually be seen). In spite of the difficulty, much has been learned from the studies that have been carried out (e.g., Markoff, Falcke & Fender 2001; Hynes et al. 2002; Ueda et al. 2002; Chaty et al. 2003; Fuchs et al. 2003;

Markoff & Nowak 2004; Markoff, Nowak & Wilms 2005; Yuan, Cui & Narayan 2005).

The broadband SED of microquasars is usually composed of several distinct components. Very roughly, at radio frequencies, the spectrum can be described by a power law, which may have either positive or negative frequency dependence. The emission is generally thought to be synchrotron radiation from relativistic electrons in the jets, which may be optically thin or thick to synchrotron self-absorption (Hjellming & Han 1995; Fender 2006). Such a synchrotron spectrum could extend up to infrared/optical frequencies in some cases (e.g., Chaty et al. 2003; Migliari et al. 2007). From optical to soft X-ray frequencies, the spectrum takes on a blackbody-like shape, which is usually viewed as the signature of an optically thick, geometrically thin accretion disc (review by Liang 1998). It is seen to peak at different frequencies for different sources or even for a given source at different fluxes; the latter has been interpreted as being related to the movement of the inner edge of the disc (e.g., Esin, McClintock & Narayan 1997). From hard X-ray to soft gamma-ray frequencies, the spectrum can, once again, be roughly described by a power law, which rolls over at some characteristic frequency under certain circumstances. It is

\* E-mail: xuey@physics.purdue.edu

† E-mail: wuxb@vega.bac.pku.edu.cn

‡ On sabbatical leave from the Department of Physics, Purdue University; e-mail: cui@physics.purdue.edu

generally modelled as Compton upscattering of soft photons by energetic electrons in an optically-thin configuration (Liang 1998).

The physical origin of Comptonizing electrons is still not entirely clear. They may be thermal electrons associated with advection dominated accretion flows (ADAF; see, e.g., Narayan, Mahadevan & Quataert 1998) or magnetic flares (e.g., Poutanen & Fabian 1999) above the thin disc. Over the years, intense efforts have been made to fit the X-ray spectrum of microquasars in the so-called low-hard state with models that include optically-thick emission from the thin disc and a Comptonized emission from some ‘corona’. The most successful and physically self-consistent models all seem to prefer a geometry that consists of an inner (roughly) spherical corona plus an outer thin disc (e.g., Dove, Wilms & Begelman 1997; Esin et al. 1997). Alternatively, the Comptonizing electrons may be non-thermal in nature (e.g., Zdziarski et al. 2001; Titarchuk & Shrader 2002). This is thought to be particularly relevant to the so-called high-soft state of microquasars (Grove et al. 1998). A promising place to accelerate electrons to the required energies is the jets, as in the case of AGN and GRBs, although the electrons could also be associated with the accretion flows. The broadband SED has proven to be a valuable tool for assessing the roles of jets and accretion flows in microquasars, as well as the coupling between the two (Yuan et al. 2005).

In this work, we examined two microquasars, XTE J1550–564 and H 1743–322, whose jets have been directly imaged at both radio and X-ray frequencies (Corbel et al. 2002, 2005), mainly to gain insights into the roles of the jets and accretion flows in microquasars. The broadband SED of the jets allowed us to assess the contribution of jets to the overall SED in a relatively model-independent manner. Moreover, modelling the jet SED helped constrain the properties of radiating electrons in the jets and thus reduced degeneracy in the modelling of the overall SED of the source. We also studied the spectral evolution of the sources during outburst and the correlation between the observed radio and X-ray variabilities.

## 2 X-RAY DATA

### 2.1 *Chandra* Data

We used the *Chandra* data to constrain the X-ray emission of the jets. We searched the *Chandra* archival database and found a total of 14 observations of XTE J1550–564 and 7 observations of H 1743–322, respectively, all taken with the ACIS detector (and some also with the HETG inserted). Since we are only interested in imaging observations here, we eliminated the ones taken in the continuous clocking mode. The remaining observations are shown in Table 1, along with references to the published works based on these observations.

For this work, we chose to re-analyse all the data in a consistent manner. We used the standard *CIAO* analysis package (version 3.3), along with the corresponding calibration database (CALDB 3.2.0), and followed the *CIAO* Science Threads<sup>1</sup> in constructing the images and spectra. We used the *CIAO* script *specextract* to extract the X-ray spectra of the jet ‘blobs’ seen, with appropriate regions for the source (circle) and background (annulus). The script produces spectra for the total and background emission, as well

**Table 1.** Log of the *Chandra* observations

ObsID	MJD (Start time)	UT Date (Start time)	Jet(s) <sup>a</sup> Detected	Ref.
XTE J1550–564				
679	51704.49	06/09/2000	E	1,2
1845	51777.36	08/21/2000	E	1,2,3
1846	51798.20	09/11/2000	E	1,2,3
3448	52344.62	03/11/2002	E,W	1,3,4
3672	52444.38	06/19/2002	W	3,4
3807	52541.83	09/24/2002	W	3
4368	52667.19	01/28/2003	W	3
5190	52935.30	10/23/2003	W	3
H 1743–322				
4565	53047.85	02/12/2004	E,W	3,5
4566	53088.74	03/24/2004	E,W	3,5
4567	53091.26	03/27/2004	E,W	3,5

References: (1) Corbel et al. (2002); (2) Tomsick et al. (2003); (3) Corbel et al. (2006); (4) Kaaret et al. (2003); (5) Corbel et al. (2005).

Note: <sup>a</sup> E=Eastern and W=Western.

as the corresponding *rmf* and *arf* files for subsequent spectral modelling. We carried out the initial modelling of the spectra in XSPEC v12.2.0ba (Arnaud 1996).

Due to the low count rates of the jet ‘blobs’, the data do not offer a good constraint on interstellar absorption. In all cases, we fixed the hydrogen column density at the line-of-sight values ( $N_H = 8.97$  and  $7.21 \times 10^{21} \text{ cm}^{-2}$  for XTE J1550–564 and H 1743–322, respectively; Dickey & Lockman 1990). For both sources, the X-ray spectrum (in the range of 0.3–8 keV) of the jet emission can be fitted satisfactorily with a power law, where the  $\chi^2$  statistics with standard weighting was employed for the rebinned spectra of jet ‘blobs’ with more than 100 counts and the  $\chi^2$  statistics with Churazov weighting (Churazov et al. 1996) was employed for the unbinned spectra of those with less than 100 counts (note that Churazov weighting is recommended by XSPEC for analysing a spectrum with very low counts). The results are summarized in Table 2. We emphasize that our goal of spectral modelling here is to get a rough idea about the spectral behavior of the jet ‘blobs’. The statistics is poor, especially in the case of H 1743–322, but it is interesting to note that the jet spectrum of H 1743–322 seems to be harder than that of XTE J1550–564. For each source, the photon indices of the jet ‘blobs’ seen are consistent with being the same (within uncertainties). To derive the intrinsic SED of a jet ‘blob’, we de-absorbed the raw count spectrum, using the photoelectric absorption cross sections of Morrison & McCammon (1983), and unfolded it.

### 2.2 *RXTE* Data

We used the *RXTE* data to obtain the X-ray SED of the *total* emission. XTE J1550–564 underwent major outbursts during 1998–2000 and H 1743–322 during 2003–2005. We analysed a series of archival *RXTE* observations taken of them during their respective outbursts. For XTE J1550–564, we selected more observations during the times of significant spectral variability (e.g., the rising phase of the 1998/1999 outburst; Cui et al. 1999) and less when the spectral variability of the source is less pronounced (e.g., the latter portion of the 1998/1999 outburst), based on the work of Sobczak et al. (2000). For H 1743–322, we selected as many observations as

<sup>1</sup> see <http://asc.harvard.edu/ciao/threads/index.html>

**Table 2.** Spectral parameters for the resolved jet ‘blobs’

ObsID	Jet Blob	Number of Counts <sup>a</sup>	Photon Index	Norm <sup>b</sup>
XTE J1550–564				
679	E	12	$1.7^{+1.2}_{-0.8}$	$4.2^{+1.0}_{-0.7}$
1845	E	24	$1.6^{+0.8}_{-0.6}$	$1.5^{+0.8}_{-0.6}$
1846	E	28	$1.6^{+0.9}_{-0.7}$	$1.9^{+0.8}_{-0.7}$
3448	E	34	$2.1^{+0.8}_{-0.7}$	$0.6^{+0.4}_{-0.3}$
	W	415	$1.74 \pm 0.18$	$5.0^{+0.9}_{-0.8}$
3672	W	251	$1.73 \pm 0.25$	$4.3^{+1.0}_{-0.9}$
3807	W	200	$1.93^{+0.29}_{-0.27}$	$2.9 \pm 0.7$
4368	W	113	$2.01^{+0.47}_{-0.39}$	$1.9^{+0.7}_{-0.6}$
5190	W	134	$1.98^{+0.36}_{-0.35}$	$1.1^{+0.4}_{-0.3}$
H 1743–322				
4565	E	28	$0.7 \pm 0.6$	$13.5^{+3.7}_{-3.5}$
	W	5	$0.5^{+0.8}_{-1.0}$	$2.1^{+3.3}_{-2.0}$
4566	E	15	$0.6^{+0.5}_{-0.6}$	$6.3^{+3.0}_{-3.1}$
	W	17	$0.3^{+1.0}_{-0.9}$	$3.6^{+3.3}_{-2.9}$
4567	E	27	$0.6^{+0.6}_{-0.8}$	$6.2^{+3.5}_{-3.0}$
	W	17	$0.2^{+0.5}_{-0.7}$	$3.1^{+3.2}_{-2.9}$

<sup>a</sup> Number of counts (background-subtracted) in the 0.3–8 keV energy range.

<sup>b</sup> For XTE J1550–564, Norm is in the unit of  $10^{-5}$  photons  $\text{keV}^{-1} \text{cm}^{-2} \text{s}^{-1}$  at 1 keV; for H 1743–322, Norm is in the unit of  $10^{-7}$  photons  $\text{keV}^{-1} \text{cm}^{-2} \text{s}^{-1}$  at 1 keV.

necessary to make sure that the spectral evolution of H 1743–322 is adequately covered throughout each of its outbursts.

We followed our usual procedure to reduce and analyse the PCA and HEXTE data collected in the standard modes (e.g., Cui 2004, Xue & Cui 2005)<sup>2</sup>. The data were reduced with *FTOOLS* 5.2. A PCA or HEXTE spectrum consists of separate spectra from individual detector units that were in operation. In deriving the PCA spectra, we only used data from the first xenon layer of each detector unit (which is best calibrated). To estimate the PCA background, we used the background model for bright sources (`pca_bkgd_cmbrightvle_eMv20030330.mdl`).

For each *RXTE* observation, we jointly fitted the PCA and HEXTE spectra with a model that consists of a multi-color disc (‘diskbb’ in XSPEC) and a power law with high-energy cutoff, taking into account the interstellar absorption. We also introduced an additional multiplicative factor to account for any uncalibrated difference in the overall throughput among the individual detector units between the PCA and HEXTE. We limited the PCA data to 3–30 keV and the HEXTE data to 15–200 keV and added 1% systematic uncertainty to the data. In some cases, we still needed an additional Gaussian component to achieve statistically acceptable fits, with its centroid at about 6–7 keV. The feature might be real (e.g., iron fluorescence line) or an artefact due to inaccuracy in the calibration around the xenon L edge (at  $\sim 4.78$  keV) and/or inadequacy of the model (in the overlapping region of the two main components). Here, we are only interested in using the best-fitting model to unfold each observed (count) spectrum to derive the corresponding photon spectrum for further modelling.

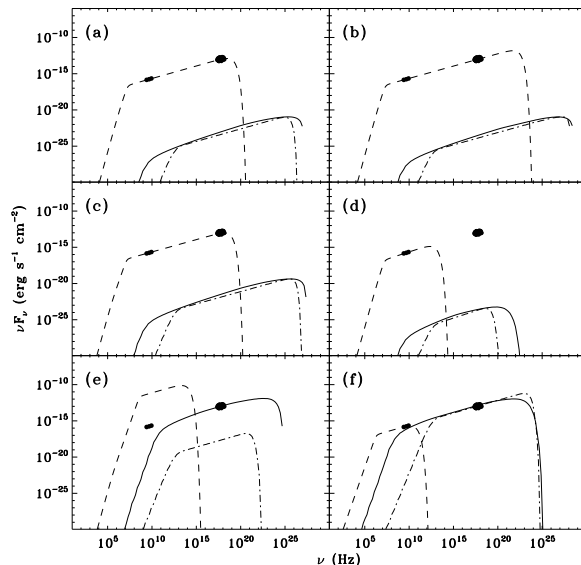


**Figure 1.** Spectral energy distribution of the western ‘blob’ in the jets of XTE J1550–564. The radio measurements were made with ATCA on MJD 52339 (Corbel et al. 2002). The X-ray measurements were made with *Chandra* on MJD 52344. The dashed, solid, and dash-dot lines show contributions from the synchrotron, SSC, and IC/CMB components, respectively. See Table 3 for model parameters for each case.

### 3 JET EMISSION

#### 3.1 XTE J1550–564

A broadband SED of the western ‘blob’ of XTE J1550–564 is shown in Fig. 1. The X-ray data were taken from the *Chandra* observation conducted on 2002 March 11 (ObsID 3448; see Table 1). One important caveat is that the radio and X-ray measurements were not made simultaneously. In fact, they were made five days apart! This is relevant because the jet emission may be variable on a time-scale of days. With this caveat in mind, we proceeded with the assumption that the western ‘blob’ did *not* vary appreciably at radio and X-ray frequencies in this case. We modelled the jet SED with a homogeneous synchrotron model (see Xue, Yuan & Cui 2006 for details), as well as with an inverse Compton (IC) scattering model. For the latter, we estimated contributions from different sources of seed photons separately. We considered synchrotron self-Compton (SSC) scattering and IC scattering off the cosmic microwave background photons (IC/CMB). For low mass X-ray binaries, the photon field of the accretion disc or of the companion star is probably much less important for the IC process in the jets.

From the *Chandra* X-ray image, we estimated the diameter of the western ‘blob’ to be roughly  $3''$  (though it is not exactly of spherical shape). Adopting the distance of  $d = 5.3$  kpc (Orosz et al. 2002), we have the size of the emitting ‘blob’  $r \sim 1 \times 10^{17}$  cm. Corbel et al. (2002) estimated the apparent velocities of both eastern and western ‘blobs’, roughly 1.0 and 0.6  $c$ , respectively. Assuming that the ‘blobs’ were ejected directly opposite to each other with the same velocity, we found that the actual velocity was about 0.8  $c$  and the inclination angle of the jet (with respect to the line of sight) about  $72^\circ$ . The latter is compatible with the optical measurements (Orosz et al. 2002). Therefore, the Doppler factors

<sup>2</sup> also see [http://heasarc.gsfc.nasa.gov/docs/xte/recipes/cook\\_book.html](http://heasarc.gsfc.nasa.gov/docs/xte/recipes/cook_book.html)

**Table 3.** Model parameters for the western jet ‘blob’ in XTE J1550–564

Case Number	$B$ (Gauss)	$E_{\text{tot}}/m_e c^2$ ( $\text{cm}^{-3}$ )	$\gamma_{\text{max}}$	$p$
(a)	0.016	25.1	$1.6 \times 10^7$	2.31
(b)	0.032	79.5	$5.0 \times 10^8$	2.32
(c)	0.002	$1.2 \times 10^3$	$3.0 \times 10^7$	2.32
(d)	0.032	0.06	$1.0 \times 10^4$	2.20
(e)	0.003	$4.0 \times 10^5$	$1.0 \times 10^5$	2.30
(f)	$8.0 \times 10^{-9}$	$1.5 \times 10^{11}$	$1.6 \times 10^6$	2.30

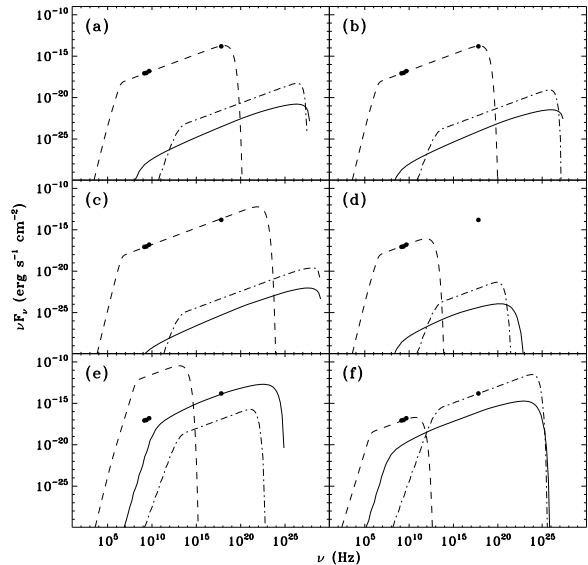
of the eastern and western ‘blobs’ are roughly 0.8 and 0.5, respectively. It should be noted that the velocity of the ‘blobs’ is thought to be much larger early on (Hannikainen et al. 2001). For subsequent modelling, we fixed the Doppler factor of the western ‘blob’ at  $\delta = 0.5$ . Moreover, we fixed the minimum Lorentz factor of electron  $\gamma_{\text{min}}$  at 10, which is sufficiently low as not to affect the conclusions. The remaining parameters in the model are: spectral index of electron  $p$ , maximum Lorentz factor of electron  $\gamma_{\text{max}}$ , energy density of electron  $E_{\text{tot}}$ , and magnetic field  $B$ .

Fig. 1 also shows representative fits to the data, with the corresponding model parameters summarized in Table 3. In general, the jet SED can be fitted well with synchrotron emission alone. We found that the electron spectral index ( $p$ ) is well constrained, in the range of 2.28–2.32, but other parameters are much less so,  $B$  in the range of 0.001–0.050 G,  $\gamma_{\text{max}} \gtrsim 1.26 \times 10^7$ , and  $E_{\text{tot}}/m_e c^2$  in the range of 20–32000  $\text{cm}^{-3}$ , due partly to significant degeneracy in the fits. The best-fitting  $p$  is 2.315, which is in good agreement with Corbel et al. (2002). In such cases (a–c), the IC (either SSC or IC/CMB) contribution to the measured fluxes is negligible. We also attempted to fit the radio data with synchrotron emission and the X-ray data with IC emission but failed to find any solutions. Cases (d–f) in Fig. 1 show examples of the fits. While Case (f) appears to show a reasonable fit, the magnetic field required would be  $8.0 \times 10^{-9}$  G, which is unrealistically small for jets in microquasars.

### 3.2 H 1743–322

Similarly, we modelled a broadband SED of the eastern ‘blob’ of H 1743–322, as shown in Fig. 2. In this case, we estimated the diameter of the ‘blob’ to be roughly  $3.2''$ , based on the *Chandra* X-ray image, which corresponds to a linear size of  $r \sim 2 \times 10^{17}$  cm, if we assume a distance of 8.0 kpc for the source. Corbel et al. (2005) found a solution to the intrinsic velocity of the ‘blobs’ ( $v = 0.79 c$ ) and the inclination angle of the jet ( $\theta = 73^\circ$ ), which would imply that the Doppler factor of the eastern ‘blob’ is  $\delta = 0.8$ . We fixed  $\delta$ , as well as the minimum Lorentz factor of the emitting electrons (at  $\gamma_{\text{min}} = 10$ ) in the fits. Because the quality of the data is not as good for H 1743–322 as for XTE J1550–564, we also fixed the electron spectral index ( $p = 2.20$ ; Corbel et al. 2005).

Fig. 2 also shows representative fits to the data, with the corresponding model parameters summarized in Table 4. Like in the case of XTE J1550–564, the jet SED can, in general, be accounted for by synchrotron emission alone (see Cases (a–c)). We also found that the X-ray emission of the jet could not be explained by the IC emission either, were the observed radio fluxes attributed to synchrotron emission (see Cases (d–f)). An apparent good fit was achieved, as shown in Case (f), but the required magnetic field would be as small as  $6.0 \times 10^{-9}$  G, which is, again, unrealistic.

**Figure 2.** As in Fig. 1, but for the eastern ‘blob’ in the jets of H 1743–322 on MJD 53047. See Table 4 for model parameters for each case.**Table 4.** Model parameters for the eastern jet ‘blob’ in H 1743–322

Case Number	$B$ (Gauss)	$E_{\text{tot}}/m_e c^2$ ( $\text{cm}^{-3}$ )	$\gamma_{\text{max}}$	$p$
(a)	$4.0 \times 10^{-4}$	344.0	$5.0 \times 10^7$	2.20
(b)	0.001	55.0	$2.5 \times 10^7$	2.20
(c)	0.005	71.0	$1.0 \times 10^9$	2.20
(d)	0.001	0.25	$2.5 \times 10^4$	2.20
(e)	0.001	$9.9 \times 10^4$	$1.0 \times 10^5$	2.20
(f)	$6.0 \times 10^{-9}$	$1.7 \times 10^9$	$2.5 \times 10^6$	2.20

## 4 TOTAL EMISSION: JET CONTRIBUTION

It is generally thought that radio emission from microquasars is due entirely to the jets. A natural question is then how much the jets contribute to emission at higher frequencies. The answer is invariably model-dependent due to the lack of detailed understanding of the formation of the jets and of the coupling between the jets and accretion flows. Here, we attempted to address the issue by using some of the results obtained in the previous section.

Fig. 3 shows the two best broadband SEDs of XTE J1550–564 in our sample, corresponding to two different spectral states (see discussion in § 5). Assuming that the synchrotron-emitting electrons follow the same spectral energy distribution for all (resolved or unresolved) ‘blobs’ in the jets (see evidence in Table 2), we fixed  $p = 2.32$  and  $\gamma_{\text{max}} = 5.0 \times 10^8$ , based on a solution for the 2002 western ‘blob’ (as shown in Fig. 1(b)). We also fixed the Doppler factor at  $\delta = 0.5$  and the radius of the emitting region at  $r = 1 \times 10^{10}$  cm. A sufficiently small  $r$  was adopted because the emission from the jets is likely dominated by optically-thick synchrotron emission from unresolved components at the core (i.e., close to the black hole). We should note that the choice of the parameter values does not affect our general conclusions (see below). The only remaining free parameters are  $B$  and  $E_{\text{tot}}$ .

We fitted the radio data with the synchrotron model. Some

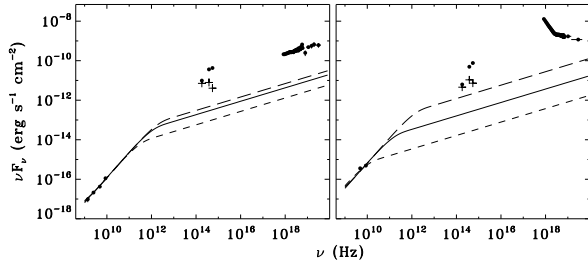


**Figure 3.** Spectral energy distribution of the total emission from XTE J1550–564 in the low-hard state (*left*) and the transitional state (*right*). The filled circles show simultaneous/contemporaneous data from radio (Corbel et al. 2001), IR/optical (Jain et al. 2001), and X-ray measurements taken around MJD 51696.47 (*left*) and MJD 51665.40 (*right*), respectively. Note that the filled circles and pluses at the IR/optical frequencies correspond to extinction corrections with  $A_V = 4.75$  (Orosz et al. 2002) and  $A_V = 2.2$  (Sánchez-Fernández et al. 1999), respectively, due to the uncertainty in the interstellar extinction for the source. The short-dashed, solid, and long-dashed lines show plausible solutions of the synchrotron model, *left*: ( $B = 1778.7$  G,  $E_{tot}/m_e c^2 = 1.1 \times 10^{16}$  cm $^{-3}$ ), ( $B = 6311.3$  G,  $E_{tot}/m_e c^2 = 4.5 \times 10^{15}$  cm $^{-3}$ ), and ( $B = 11223.3$  G,  $E_{tot}/m_e c^2 = 2.8 \times 10^{15}$  cm $^{-3}$ ); *right*: ( $B = 56.2$  G,  $E_{tot}/m_e c^2 = 1.0 \times 10^{18}$  cm $^{-3}$ ), ( $B = 891.5$  G,  $E_{tot}/m_e c^2 = 1.0 \times 10^{17}$  cm $^{-3}$ ), and ( $B = 7945.5$  G,  $E_{tot}/m_e c^2 = 2.0 \times 10^{16}$  cm $^{-3}$ ), respectively, with  $p = 2.32$  and  $\gamma_{max} = 5.0 \times 10^8$  fixed for all cases. Note that all plausible solutions fall between the long-dashed and short-dashed lines.

representative solutions are shown in Fig. 3. The spectral break at  $\sim 10^{11-12}$  Hz marks the transition between the optically-thick and optically-thin synchrotron regimes. We note that no solutions were found under the condition of equipartition between the electrons and the magnetic field, which is in agreement with Wang, Dai & Lu (2003). One thing that seems clear is that the synchrotron radiation from the jets contributes little to the observed optical and X-ray emission, at least in these two particular cases (when the source was relatively bright during the 2000 outburst). This conclusion does not appear to be sensitive to the adopted values of  $p$  and  $\gamma_{max}$ , because we also experimented with other values.

Similarly for H 1743–322, we carried out similar modelling of the two best SEDs of the total emission in our sample, which are shown in Fig. 4, also corresponding to two different spectral states. In this case, we fixed the following parameters:  $\delta = 0.8$ ,  $r = 1 \times 10^{10}$  cm, and  $p = 2.20$ . Representative solutions are also shown in Fig. 4. Again, we found no solutions under the condition of equipartition between the electrons and the magnetic field. The results support the conclusion that, while the jets can probably account for 100% of the observed radio emission, they contribute little to the observed emission at higher frequencies, when the source is relatively bright.

Where does the bulk of the X-ray emission come from then? We speculate that it originates mostly from accretion flows, as for XTE J1118+480 (Yuan et al. 2005). Indeed, when we followed the usual empirical approach of modelling the X-ray spectrum, with a power law (plus a high-energy rollover for the low-hard state), which approximates an unsaturated Comptonized spectrum, and a multi-color disc component (when needed), we found that the model can adequately fit the data. In principle, inverse Compton scattering could also take place in the jets and the Comptonized photons could contribute to the observed hard X-ray emission (Giannios 2005). However, we have shown in § 3 that the IC emission from the jets is likely to play a negligible role, at least for XTE J1550–564 and H 1743–322.

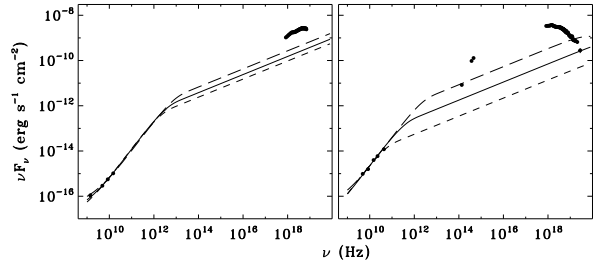


**Figure 4.** As in Fig. 3, but for H 1743–322 in the low-hard state (*left*) and the transitional state (*right*). The data were taken around MJD 52729.79 (*left*) and MJD 52733.78 (*right*), respectively, *left*: radio data from Rupen et al. (2003), *right*: both radio and IR/optical data from McClintock et al. (2007). The short-dashed, solid, and long-dashed lines show plausible solutions of the synchrotron model, *left*: ( $B = 7945.5$  G,  $\gamma_{max} = 1.4 \times 10^7$ ,  $E_{tot}/m_e c^2 = 7.9 \times 10^{15}$  cm $^{-3}$ ), ( $B = 14129.3$  G,  $\gamma_{max} = 1.4 \times 10^8$ ,  $E_{tot}/m_e c^2 = 3.2 \times 10^{16}$  cm $^{-3}$ ), and ( $B = 31632.0$  G,  $\gamma_{max} = 4.0 \times 10^6$ ,  $E_{tot}/m_e c^2 = 8.9 \times 10^{14}$  cm $^{-3}$ ); *right*: ( $B = 199.5$  G,  $\gamma_{max} = 3.2 \times 10^6$ ,  $E_{tot}/m_e c^2 = 1.3 \times 10^{17}$  cm $^{-3}$ ), ( $B = 1412.6$  G,  $\gamma_{max} = 1.0 \times 10^6$ ,  $E_{tot}/m_e c^2 = 1.1 \times 10^{16}$  cm $^{-3}$ ), and ( $B = 8913.2$  G,  $\gamma_{max} = 1.0 \times 10^5$ ,  $E_{tot}/m_e c^2 = 4.5 \times 10^{14}$  cm $^{-3}$ ), respectively, with  $p = 2.20$  fixed for all cases.

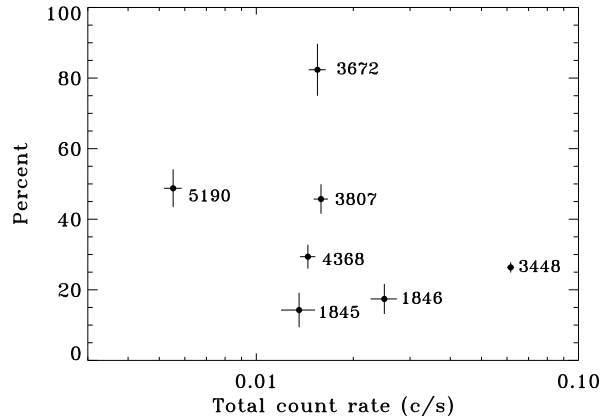


**Figure 5.** Contribution of the resolved jet ‘bolbs’ in XTE J1550–564 to the total observed X-ray emission, with observation ID shown for each point. All the count rates were background-subtracted and computed within the energy range of 0.3–8 keV. Note that each data point only shows a *lower* limit on the overall contribution of the jets (see text).

On the other hand, as the source becomes fainter, the contribution of the jets to the higher-frequency emission is thought to increase and perhaps eventually dominate (Yuan & Cui 2005). To investigate whether there is observational evidence to support it, we computed the ratio of the summed count rate, of all resolved jet ‘blobs’ to the total count rate (of the core and ‘blobs’) directly from the *Chandra* images of XTE J1550–564. The quantity should represent a *lower* limit on the fractional contribution of the jets to the total emission, since there may be unresolved ‘blobs’ along the jets or at the core. Fig. 5 show the results at various intensities of the source. It is clear that the jet emission can indeed account for the bulk of, e.g., X-ray emission, when the source is relatively faint. We were not able to repeat the analysis for H 1743–322 due to the lack of statistics in this case.

## 5 SPECTRAL EVOLUTION

The spectral evolution of microquasars is often described empirically in terms of transitions between discrete spectral states (reviews by, e.g., Tanaka & Lewin 1995; Liang 1998; Homan & Belloni 2005; McClintock & Remillard 2006). However, different authors often define the states differently, which makes discussion and comparison of observational results difficult. In this work, we define the low-hard state (LHS) as one in which the SED of the source peaks at  $\sim 100$  keV and the high-soft state (HSS) as one in which the SED peaks at  $\sim 1$  keV. From the theoretical point of view, LHS thus defined represents a physical configuration in which the X-ray spectrum is due entirely to Comptonized emission (e.g., from hot accretion flows), while HSS represents one in which the X-ray spectrum is due entirely to optically-thick emission (from cold accretion flows). As such, they would correspond to the most diametrically opposed theoretical scenarios for microquasars. Strictly speaking, therefore, one is likely to observe a source only in a quasi LHS or HSS. During a transition between the two states, the source is expected to show ‘intermediate’ properties that one often observes in the ‘intermediate state’ or ‘very high state’. For transient microquasars, it is also necessary to introduce the ‘quiescent state’, which may or may not be a simple extension of the LHS toward low fluxes.

### 5.1 XTE J1550–564

Within the established context, we now discuss the observed spectral evolution of XTE J1550–564 during outbursts in 1998–2000. We examined the 2000 outburst first, because the outburst has a relatively simple profile and it was well covered observationally both during its rising and decaying phases. Fig. 6 shows representative SEDs of XTE J1550–564 during the 2000 outburst, along with an overview of the outburst based on the ASM data. The SEDs clearly show spectral softening and hardening of the source as the outburst proceeds. More specifically, it is apparent that the source underwent an LHS-to-HSS transition (the shape of the SED goes from being high-frequency peaked to low-frequency peaked) somewhere between observations taken on MJD 51658.60 and on MJD 51662.17 (see Panel I) during the rising phase of the outburst and an HSS-to-LHS transition somewhere between observations taken on MJD 51678.45 and on MJD 51682.31 (see Panel II) during the decaying phase. This is at odds with the description of states during the same outburst by Corbel et al. (2001), who implied that the HSS was never reached in the outburst (see Fig. 1 of their paper). Even with such a large uncertainty in the timing of the transitions, we can still see evidence for spectral hysteresis associated with the rise and fall of the outburst, in the sense that the transitions seem to have occurred at different fluxes. The concept of spectral hysteresis is not new (Miyamoto et al. 1995; Nowak, Wilms & Dove 2002; Maccarone & Coppi 2003; Zdziarski et al. 2004). However, it can be confusing to discuss hysteresis without a clear definition of the states involved and a way to quantify the timing of the transitions. We will elaborate on this point below.

We repeated the analysis for the 1998/1999 outburst of XTE J1550–564, which is much stronger in its peak magnitude. Fig. 7 shows the representative SEDs, along with the ASM light curve. Spectral variability is also apparent throughout the outburst. It is interesting to note that in this case the source never seems to have reached the HSS during the 1998 sub-outburst (corresponding to the first ‘hump’ in the ASM light curve), judging from the shape of the SEDs. Instead, the SED of the source evolved from a typical

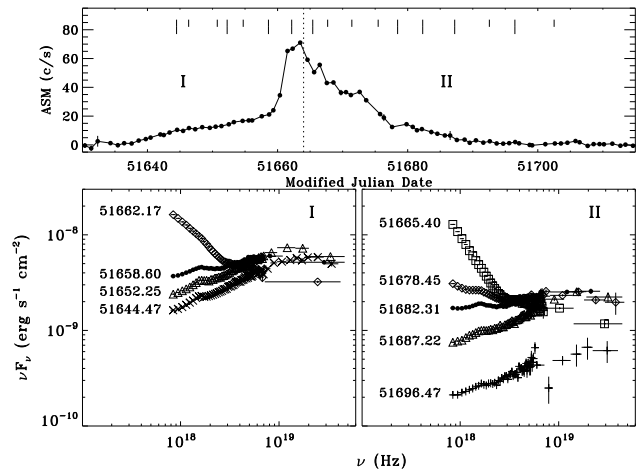


**Figure 6.** *Top:* Daily-averaged summed-band (1.5–12 keV) ASM/RXTE light curve of XTE J1550–564 in 2000, with the rising and decaying phases marked for comparison. Both short and long vertical lines indicate the times of the pointed PCA/HEXTE observations we chose in this work, with long vertical lines indicating representative SEDs shown in the *Bottom* panels. *Bottom:* Representative SEDs for the rising and decaying phases of the outburst, respectively. The start time (in MJD) of each observation selected is indicated.

LHS shape to an intermediate one that peaks at a significantly lower energy but without a dominant soft component (which defines the HSS SED). The soft component eventually emerged during the decaying phase of the sub-outburst (e.g., in the observation taken on MJD 51121.00, see Panel II). Spectral softening continued during the rising phase of the 1999 sub-outburst (corresponding to the second ‘hump’ in the ASM light curve). The source finally reached the HSS at the peak of the sub-outburst (in the observation taken on MJD 51191.49, see Panel III). During the decaying phase of the sub-outburst, the source went through an HSS-to-LHS transition (see Panel IV), which is similar to the 2000 outburst but seems to have occurred at lower fluxes (comparing Panel II in Fig. 6 and Panel IV in Fig. 7). This supports the suggestion that spectral states cannot be uniquely determined by mass accretion rate (Homan et al. 2001).

The SEDs shown have revealed that the HSS differs significantly from the ‘intermediate’ period, which lasted for quite a long time during the 1998/1999 outburst, although the ‘intermediate’ SEDs seem to bear more resemblance to the HSS SED than the LHS SED. Maccarone & Coppi (2003) reported spectral hysteresis associated with the first sub-outburst, based on the ASM light curve and hardness ratios. It is clear, however, that that phenomenon is very different from the one that we are discussing here (i.e., spectral hysteresis associated with transitions between LHS and HSS), because the source was in constant transition and never in fact reached HSS during the sub-outburst. This example illustrates the difficulty in comparing results in the literature in the absence of a clear definition of the states.

### 5.2 H 1743–322

The representative SEDs of H 1743–322 are shown in Figs. 8–10 for its 2003, 2004, and 2005 outbursts, respectively, along with the ASM light curves. Interestingly, the 2003 outburst also has a two-hump profile, like the 1998/1999 outburst of XTE J1550–564,

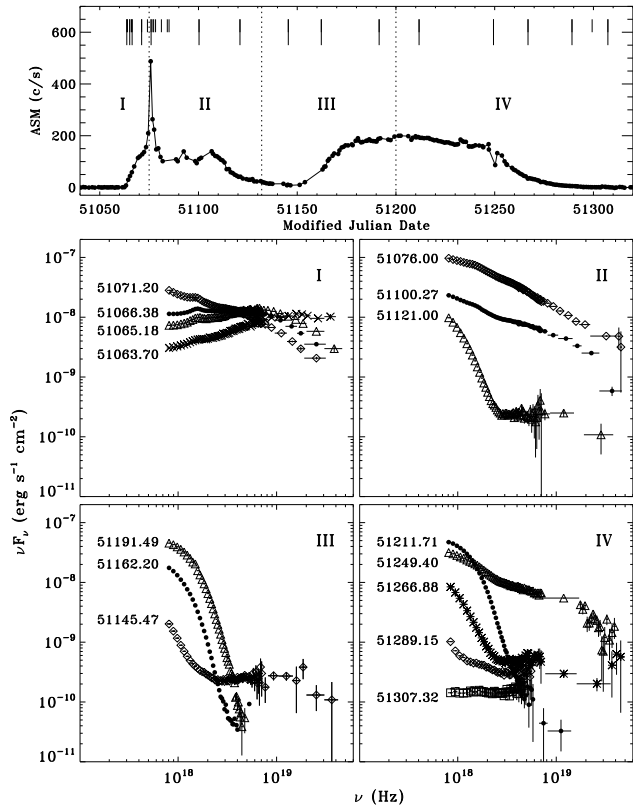


Figure 7. As in Fig. 6, but for XTE J1550–564 in the 1998/1999 outburst.

while the 2004 and 2005 outbursts are more similar in shape to the 2000 outburst of XTE J1550–564.

In the 2003 outburst (Fig. 8), during the rising phase of the first ‘hump’ (Panel I), no HSS was reached, although the X-ray spectrum softened continuously. During the decaying phase of the first ‘hump’ (Panel II) and the rising phase of the second ‘hump’ (Panel III), the source exhibited complicated spectral behaviors: the soft (disc) component emerged, disappeared, and re-appeared. This is probably due to the sub-structures associated with both ‘humps’. The HSS was eventually reached during the decaying phase of the second ‘hump’ (Panel IV), as indicated by the dominance of the soft component. Subsequently, the source underwent an HSS-to-LHS transition.

In the 2004 and 2005 outbursts (Figs. 9 and 10), the coverage of both rising phases is not as good. No clear LHS was observed. However, HSS-to-LHS transitions can easily be inferred, during the decaying phases. Once again, we see that a specific state transition may occur at different fluxes (comparing Panel IV in Fig. 8, Panel II in Fig. 9, and Panel II in Fig. 10).

## 6 X-RAY/RADIO CORRELATION

Finally, we used the multiwavelength data to examine correlation between the observed radio and X-ray variabilities. The correlation is of interest because it might be related to a coupling between the jets and accretion flows in microquasars (Yuan & Cui 2005). Such a coupling is a key ingredient in many models of jet formation (e.g., Falcke & Biermann 1995; Meier 2001). The radio/X-ray correlation has been studied extensively (e.g., Corbel et al. 2003; Gallo, Fender & Pooley 2003; Fender, Belloni & Gallo 2004; Xue & Cui

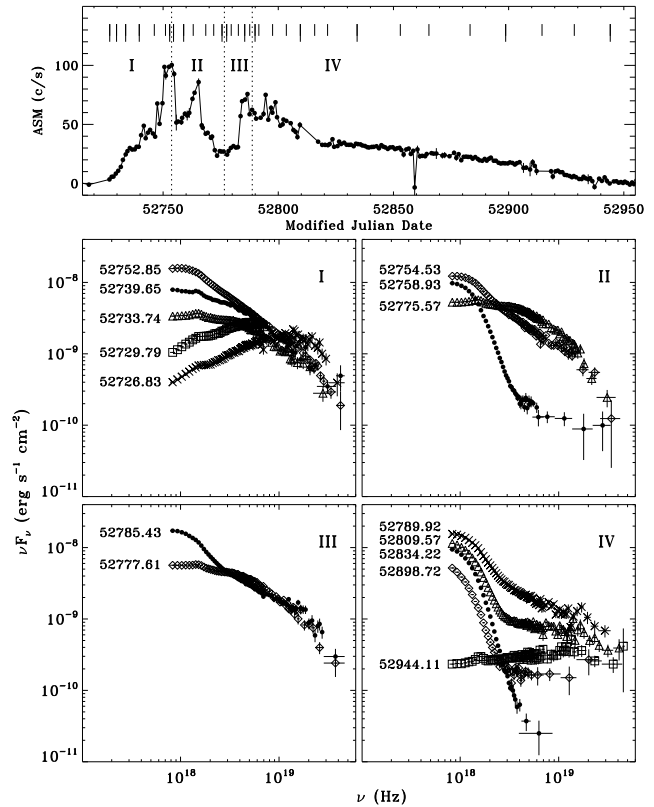


Figure 8. As in Fig. 6, but for H 1743–322 in the 2003 outburst.

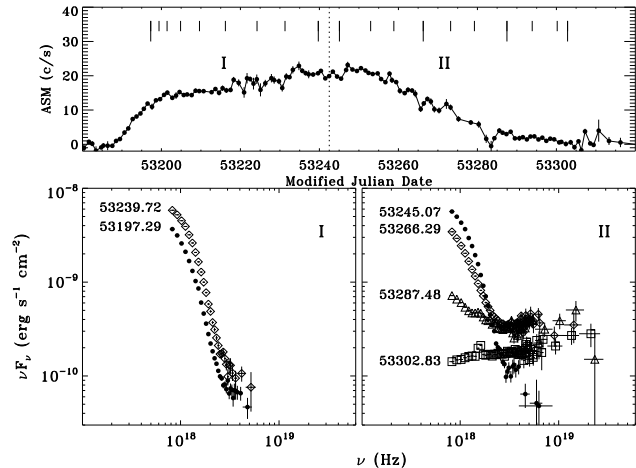
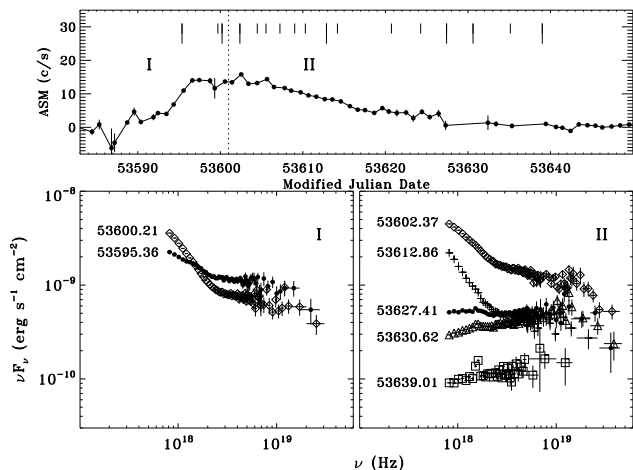


Figure 9. As in Fig. 8, but for H 1743–322 in the 2004 outburst.

2007). It was claimed that a ‘universal’ radio/X-ray correlation exists for microquasars (Gallo, Fender & Pooley 2003). However, the universality of the correlation has recently been ruled out by observations (Xue & Cui 2007). It is nevertheless apparent that for a given microquasar, radio and X-ray variabilities may, to varying degrees, be correlated (which can probably be extended to the infrared band; see Russell et al. 2007). To this end, we put together simultaneous/contemporaneous radio and X-ray measurements for XTE J1550–564. The results for H 1743–322 can be found in Xue & Cui (2007).

Fig. 11 plots radio flux measurements ( $F_R$ ), at 843, 4800, and 8640 MHz respectively, against the 2–11 keV X-ray fluxes ( $F_X$ )



**Figure 10.** As in Fig. 8, but for H 1743–322 in the 2005 outburst.

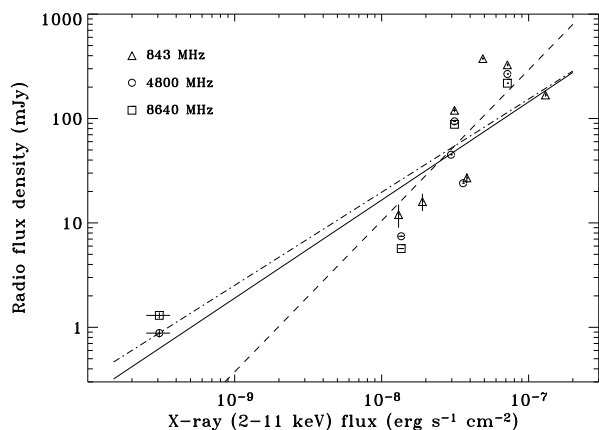


**Figure 11.** Radio/X-ray correlation in XTE J1550–564. The radio measurements at 843, 4800, and 8640 MHz (taken from Wu et al. 2002, Hannikainen et al. 2001, and Corbel et al. 2001) are shown in triangles, circles, and squares, respectively. The dashed, solid, and dash-dot lines show separately the best-fitting power laws to the data taken at 843, 4800, and 8640 MHz. Note large scatters in the fits.

of XTE J1550–564. Note that the energy range for X-ray fluxes was chosen to facilitate direct comparison with the published results (e.g., Xue & Cui 2007). Although the number of data points is quite limited, the data cover a dynamical range of over two orders of magnitude both in radio and X-ray fluxes. At the first glance, a general positive correlation is apparent. Following the literature, we then fitted the data with a power law, in the form of  $\log_{10} F_R = k \log_{10} F_X + b$ , separately for radio data at different frequencies. The results are also shown in Fig. 11. The best-fitting logarithmic slope ( $k$ ) was found to be 1.45, 0.94, and 0.89 for radio measurements at 843, 4800, and 8640 MHz, respectively. However, none of the fits is formally acceptable; large scatters are apparent.

We note that the radio/X-ray correlation is often said to be applicable only to the LHS, in which the jets are thought to be compact and steady (e.g., Corbel et al. 2001), but the radio/X-ray data used here are mostly for transitional periods between the LHS and HSS (when the jets are thought to be composed of discrete ejection events, e.g., Corbel et al. 2001), based on the definitions of the states adopted for this work. Yet, a general correlation seems to be

apparent when *all* data points are included, at least for XTE J1550–564, as shown in Fig. 11. Quantitative difference among the wavebands shows a possible spectral dependence of the correlation.

## 7 SUMMARY

We have carried out a systematic study of the SED of XTE J1550–564 and H 1743–322, and their spectral evolution during a number of major outbursts. The main conclusions of the work are summarized as follows:

(i) The results from physical modelling of the broadband SED of the resolved components of the jets support a pure synchrotron origin of the observed emission, from radio to X-ray frequencies, in XTE J1550–564 and H 1743–322. The effects of inverse Compton scattering in the jets were examined and found to be negligible. This is at variance with some of the published works (e.g., Markoff & Nowak 2004; Giannios 2005; Markoff, Nowak & Wilms 2005), which argue for a dominant role of inverse Compton scattering in the production of X-rays from microquasars based on modeling the unresolved (jets plus core) emission of the sources.

(ii) We found that the synchrotron radiation from the jets can account for 100% of the observed radio emission but seems to contribute little to the observed X-ray emission from XTE J1550–564 and H 1743–322, when the sources are relatively bright. We think that the bulk of the X-ray emission comes from the accretion flows, which is always thought to be the case. We have found observational evidence to show that the jet contribution at X-ray energies increases as the sources become fainter, and might eventually dominate in or close to the quiescent state.

(iii) We found it straightforward to define the spectral states based on the shape of SEDs. The presence of a dominant soft (disc) component distinguishes the HSS from transitional states. In the context of the adopted definitions of the spectral states, we presented clear evidence for spectral hysteresis associated with the LHS-to-HSS and HSS-to-LHS transitions associated with the rising and decaying phases of an outburst. We also showed additional evidence to support a previous suggestion that the mass accretion rate alone cannot uniquely determine spectral states.

(iv) There is a general positive correlation between the X-ray and radio fluxes in XTE J1550–564 even during the transitional states. We found evidence for a possible frequency dependence of the correlation.

## ACKNOWLEDGMENTS

We thank Feng Yuan for the use of his synchrotron utility and for helpful discussions. Y.X. wishes to thank Keith Arnaud for helpful discussions on part of the XSPEC modelling. W.C. also wishes to thank the colleagues in the Department of Astronomy at Peking University for their hospitality during his stay there. This work has made use of data obtained through the High Energy Astrophysics Science Archive Research Center Online Service, provided by the NASA/Goddard Space Flight Center. We gratefully acknowledge financial support from the Purdue Research Foundation, from the U.S. National Aeronautics and Space Administration through the ADP grant NNX07AH43G, from the National Natural Science Foundation of China through grants 10473001 and 10525313, and from the Ministry of Education (P.R.C.) through the RFDP Grant (No. 20050001026), the Key Grant (No. 305001) and the NCET program (NCET-04-0022).

**REFERENCES**

- Arnaud K. A., 1996, *Astronomical Data Analysis Software and Systems V*, eds. Jacoby G. and Barnes J., ASP Conf. Series, vol. 101, p. 17
- Chaty S. et al., 2003, *MNRAS*, 346, 689
- Churazov E. et al., 1996, *ApJ*, 471, 673
- Corbel S. et al., 2001, *ApJ*, 554, 43
- Corbel S. et al., 2002, *Science*, 298, 196
- Corbel S. et al., 2003, *A&A*, 400, 1007
- Corbel S. et al., 2005, *ApJ*, 632, 504
- Corbel S. et al., 2006, *ApJ*, 636, 971
- Cui W., Zhang S. N., Chen W., Morgan E. H., 1999, *ApJ*, 512, L43
- Cui W., 2004, *ApJ*, 605, 662
- Cui W., 2006, *Science*, 309, 714
- Dickey J. M., Lockman F. J., 1990, *ARA&A*, 28, 215
- Dove J. B., Wilms J., Begelman M. C., 1997, *ApJ*, 487, 747
- Esin A. A., McClintock J. E., Narayan R., 1997, 489, 865
- Falcke H., Biermann P. L., 1995, *A&A*, 293, 665
- Fender R. P., 2006, in *Compact Stellar X-ray Sources*, eds. W. H. G. Lewin, M. van der Klis, (Cambridge: Cambridge Univ. Press), 381
- Fender R. P., Belloni T. M., Gallo E., 2004, *MNRAS*, 355, 1105
- Fuchs Y. et al., 2003, *A&A*, 409, L35
- Gallo E., Fender R. P., Pooley G. G., 2003, *MNRAS*, 344, 60
- Giannios D., 2005, *A&A*, 437, 1007
- Grove J. E. et al., 1998, *ApJ*, 500, 899
- Hannikainen D. et al., 2001, *Ap&SS Suppl.*, 276, 45
- Hjellming R. M., Han X., 1995, in *X-ray Binaries*, eds. W. H. G. Lewin, J. Van Paradijs, E. P. J. van den Heuvel (Cambridge: Cambridge Univ. Press), 308
- Homan J. et al., 2001, *ApJS*, 132, 377
- Homan J., Belloni T., 2005, *Ap&SS*, 300, 107
- Hynes R. I. et al., 2002, *MNRAS*, 331, 169
- Jain R. K. et al., 2001, *ApJ*, 554, L181
- Kaaret P. et al., 2003, *ApJ*, 582, 945
- Liang E. P., 1998, *Phys. Rep.*, 302, 67
- Maccarone T. J., Coppi P. S., 2003, *MNRAS*, 338, 189
- Markoff S., Falcke H., Fender R., 2001, *A&A*, 372, L25
- Markoff S., Nowak M. A., 2004, *ApJ*, 609, 972
- Markoff S., Nowak M. A., Wilms J., 2005, *ApJ*, 635, 1203
- McClintock J. E., Remillard R., 2006, in *Compact Stellar X-ray Sources*, eds. W. H. G. Lewin, M. van der Klis, (Cambridge: Cambridge Univ. Press), 157
- McClintock J. E. et al., 2007 (astro-ph/0705.1034)
- Meier D. L., 2001, *ApJ*, 548, L9
- Migliari S. et al., 2007, *ApJ*, in press (astro-ph/0707.4500)
- Mirabel I., 2004, *PThPS*, 155, 71
- Miyamoto S. et al., 1995, *ApJ*, 442, L13
- Morrison R., McCammon D., 1983, *ApJ*, 270, 119
- Narayan R., Mahadevan R., Quataert E., 1998, in *The Theory of Black Hole Accretion Discs*, eds. M. A. Abramowicz, G. Bjornsson, and J. E. Pringle (astro-ph/9803141)
- Nowak M. A., Wilms J., Dove J. B., 2002, *MNRAS*, 332, 856
- Orosz J. A. et al., 2002, *ApJ*, 568, 845
- Poutanen J., Fabian A. C., 1999, *A&A*, 306, L31
- Rupen M. P., Mioduszewski A. J., Dhawan V., 2003, *IAU Circ.* 8105, 3
- Russell D. M. et al., 2007, *MNRAS*, 379, 1401
- Sánchez-Fernández C. et al., 1999, *A&A*, 348, L9
- Sobczak G. J. et al., 2000, *ApJ*, 544, 993
- Tanaka Y., Lewin W. H. G., 1995, in *X-ray Binaries*, eds. W. H. G. Lewin, J. Van Paradijs, E. P. J. van den Heuvel (Cambridge: Cambridge Univ. Press), 126
- Titarchuk L., Shrader C. R., 2002, *ApJ*, 567, 1057
- Tomsick J. A. et al., 2003, *ApJ*, 582, 933
- Ueda Y. et al., 2002, *ApJ*, 571, 918
- Wang X. Y., Dai Z. G., Lu T., 2003, *ApJ*, 592, 347
- Wu K. et al., 2002, *ApJ*, 565, 1161
- Xue Y. Q., Cui W., 2005, *ApJ*, 622, 160
- Xue Y. Q., Cui W., 2007, *A&A*, 466, 1053
- Xue Y. Q., Yuan F., Cui W., 2006, *ApJ*, 647, 194
- Yuan F., Cui W., 2005, *ApJ*, 629, 408
- Yuan F., Cui W., Narayan R., 2005, *ApJ*, 620, 905
- Zdziarski A. A. et al., 2001, *ApJ*, 554, L45
- Zdziarski A. A. et al., 2004, *MNRAS*, 351, 791